

## Positron-annihilation study of the half-metallic ferromagnet NiMnSb: Theory

K. E. H. M. Hanssen and P. E. Mijnaerends

*Netherlands Energy Research Foundation ECN, NL-1755 ZG Petten, The Netherlands*

(Received 10 April 1986)

Calculations of the electronic structure, the Fermi surface, and the momentum density of annihilation photon pairs are presented in preparation for an experimental study of the half-metallic ferromagnet NiMnSb with the aid of the two-dimensional angular correlation of annihilation radiation technique. The band structure obtained is in good agreement with former calculations and consists of a metallic majority-spin and a semiconducting minority-spin band. The majority-spin Fermi surface consists of three  $\Gamma$ -centered hole sheets, two of which have necks at  $L$ . The different nature of the bands is clearly reflected in the spin-dependent momentum densities. From these densities a magnetic difference effect in the angular correlation can be derived which should be clearly observable with polarized positrons.

### I. INTRODUCTION

Band-structure calculations for the  $C1_b$  Heusler compounds NiMnSb and PtMnSb,<sup>1,2</sup> and other compounds in this series,<sup>3</sup> have revealed a number of unique and interesting features of the electronic structure of these materials. It was found that NiMnSb, PtMnSb, and CoMnSb, all ferromagnets, possess a metallic majority-spin band, while the minority-spin band shows a gap straddling the Fermi level, a situation typical of a semiconductor. The simultaneous occurrence of these two types of band structure within one and the same material, called half-metallic ferromagnetism, is unusual. It should lead, for example, to a 100% polarization of the conduction electrons at the Fermi level. Recent calculations by de Groot and Buschow<sup>4</sup> suggest half-metallic ferrimagnetism and antiferromagnetism for other Heusler compounds.

The interest in Heusler compounds with the  $C1_b$  structure<sup>5</sup> originated in the observation in PtMnSb of an uncommonly high magneto-optical Kerr effect at room temperature.<sup>6,7</sup> This makes PtMnSb a possible candidate for applications such as erasable magneto-optical recording.<sup>8</sup> Although the band structures of NiMnSb and PtMnSb are very similar, the large value of the magneto-optical Kerr effect found in PtMnSb is not shared by NiMnSb. According to de Groot *et al.*<sup>2</sup> the large value in PtMnSb stems from the close vicinity of the Fermi level to the  $\Gamma_4$  state at the top of the minority-spin valence band. Spin-orbit coupling splits this state into three sublevels, one of which is pushed above the Fermi level. This allows excitations in which the contributions of oppositely polarized electrons to the off-diagonal element of the dielectric tensor no longer cancel, resulting in the observed high value of the Kerr effect. In NiMnSb the distance between the Fermi level and the top of the minority-spin band is greater and hence this mechanism is not operative.

There is limited experimental information relating directly to the electronic structure of these materials. Besides the measurements of the magneto-optical Kerr effect already mentioned, ellipsometry measurements have been performed on NiMnSb and PtMnSb by van Engen<sup>9</sup> and

van der Heide *et al.*<sup>10</sup> The measured optical conductivities were in reasonable agreement with the calculated ones, based on the band structure of de Groot *et al.*,<sup>1,2</sup> but a discrepancy was found in the position of the onset of the minority-spin interband transitions in NiMnSb. In the experiments it was found to occur at 0.7 eV, i.e., 0.5 eV lower than in the calculated curves. This difference can be partially explained by spin-orbit interaction. Recent spin-polarized photoemission measurements which probe the polarization of the conduction electrons at the Fermi level suggest a band gap smaller than 0.5 eV.<sup>11</sup>

A rather direct way of investigating the electronic structure in  $\mathbf{k}$  space is to measure the angular correlation of annihilation radiation in two dimensions (2D-ACAR).<sup>12</sup> The inherent (partial) spin polarization of a positron ( $e^+$ ) beam from a radioactive source enables one to study the two electron-spin populations in a ferromagnet separately.<sup>13,14</sup> We have calculated the momentum density of annihilation photon pairs in NiMnSb in preparation for spin-polarized 2D-ACAR measurements on this material, currently in progress in our laboratory. The choice for NiMnSb in preference to PtMnSb was based on the availability of a single crystal of a reasonable quality. An additional motivation for carrying out the calculations is the presence of empty lattice sites in the  $C1_b$  structure. As known, positrons show a marked affinity to vacancies, resulting in a narrowing of the angular correlation and a general blurring of Fermi-surface-related structure.<sup>15</sup> The empty sites might be expected to perturb the measurement in a similar manner. Our calculations show that there is indeed a strong increase of the positron density and thus preferred annihilation at the empty sites. On the other hand, the momentum density for Compton scattering, which in the independent-particle model differs from that for positron annihilation in the assumption of a constant positron wave function, is not affected. Hence a comparison between the two momentum densities allows an assessment of the effects of preferred positron annihilation at the empty sites. These effects will be shown to be minimal.

This article has been organized as follows. The next section contains the results of the band-structure calcula-

tions and a discussion of the  $e^+$  distribution in the unit cell. Group theory is used to investigate the effects of crystal symmetry on the momentum density. Subsequently, the results of the calculations of the momentum densities for positron annihilation and for Compton scattering are presented. The article is concluded with a discussion of the results.

## II. CALCULATIONS

### A. Crystal structure

NiMnSb is a Heusler compound with the  $C1_b$  structure [space group  $T_d^2(F\bar{4}3m)$ ] shown in Fig. 1. This structure consists of four interpenetrating fcc sublattices with origins at the positions  $A(000)$ ,  $B(\frac{1}{4}\frac{1}{4}\frac{1}{4})$ ,  $C(\frac{1}{2}\frac{1}{2}\frac{1}{2})$ , and  $D(\frac{3}{4}\frac{3}{4}\frac{3}{4})$ . Helmholdt *et al.*<sup>16</sup> have unequivocally established the site occupancy shown in Fig. 1. The  $C$  sublattice is empty, in contrast to the situation in the  $L2_1$  structure<sup>5</sup> of the more common Heusler compounds of the type  $X_2MnY$  where it is occupied by  $X$  atoms.<sup>17</sup> Below the Curie temperature  $T_c = 756$  K the magnetic moments of  $4.0\mu_B$  situated on the Mn atoms<sup>16</sup> order ferromagnetically. The point symmetry of both the  $C1_b$  and the  $L2_1$  structures is  $T_d$ , which differs from the full cubic point group  $O_h$  by the lack of inversion symmetry.

### B. Electronic structure and positron state

Our calculations are based on a muffin-tin version of the self-consistent potentials from the augmented-spherical-wave (ASW) calculation of de Groot *et al.*<sup>1</sup> but employ the Korringa-Kohn-Rostoker (KKR) method. This avoids duplication of the time-consuming self-consistency process while providing the greater accuracy of the KKR wave functions over those produced by the ASW method. The KKR calculation included terms up to  $l=2$ . Relativistic effects were incorporated according to the scalar relativistic approximation.<sup>18</sup> A lattice constant  $a=11.187$  a.u. was used. The band structure was calculated for both spin directions at 240  $k$  points in the irreducible  $\frac{1}{48}$ th of the Brillouin zone and is shown in Fig. 2. The results are in good agreement with the ASW cal-

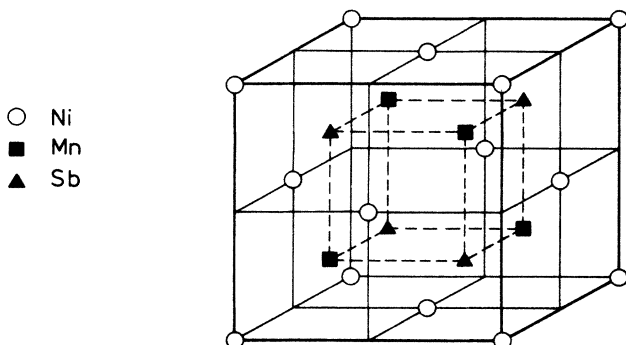


FIG. 1.  $C1_b$ -type crystal structure of NiMnSb and PtMnSb.

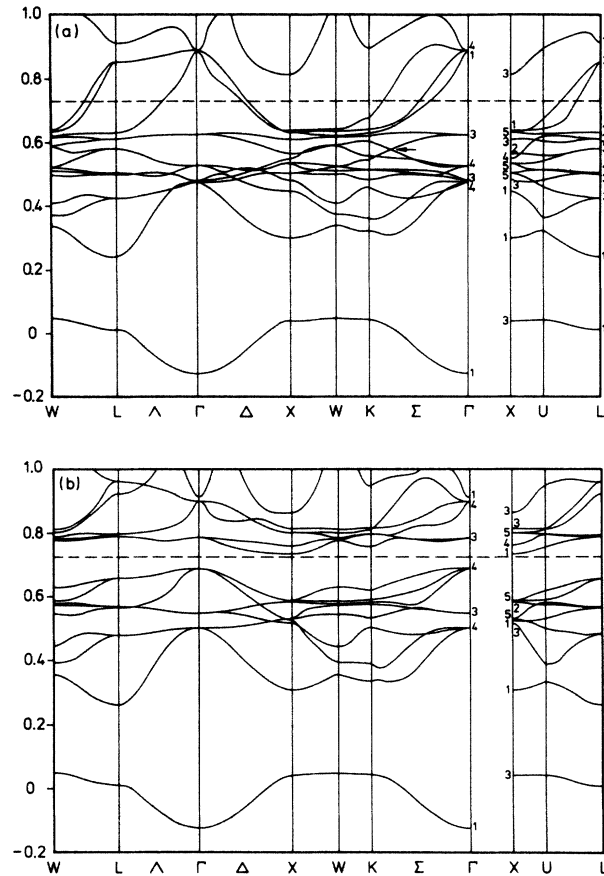


FIG. 2. Band structure for (a) the majority-spin and (b) the minority-spin electron population in NiMnSb. Symmetry labels have been assigned according to Ref. 19. Energies in Ry.

culations of de Groot *et al.*<sup>1</sup> For bands just below the Fermi level differences of about 5 mRy occur; elsewhere they increase to about 10 mRy. This is quite satisfactory in view of the different approximations in the two methods (use of a single kinetic-energy parameter for all orbitals in the ASW method and a muffin-tin potential in the KKR method). A low-lying  $s$  band of predominant Sb character was left out of Fig. 1 of de Groot *et al.* Since this band yields a major contribution to the momentum density we have included it in Fig. 2. Owing to the absence of inversion symmetry in the  $T_d$  point group, bands belonging to the same irreducible representation are under certain conditions allowed to cross.<sup>20</sup> Crossings of this nature can be seen in the majority-spin band structure along  $\Gamma K$  [see arrow in Fig. (2a)].

The total densities of states for the two spin directions have been calculated according to the analytic-quadratic method of Methfessel *et al.*<sup>21</sup> and are illustrated in Fig. 3. For the minority spin the Fermi level lies just below the conduction band, whereas in PtMnSb it is very close to the top of the valence band. This difference in position is crucial to the explanation of the large Kerr effect in PtMnSb.

The Fermi surface of the majority-spin electrons consists of three sheets as shown in Fig. 4. Band 12 gives rise

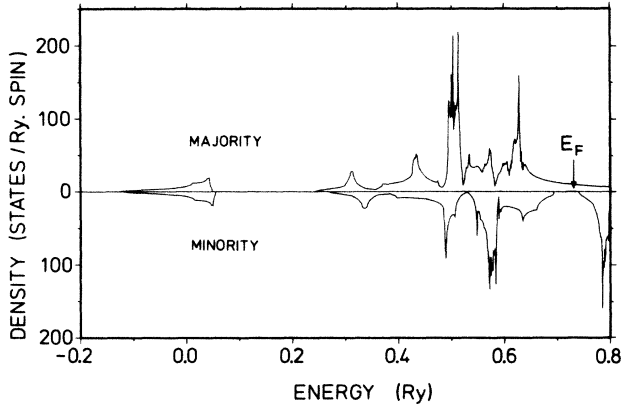


FIG. 3. Total density of states of NiMnSb for the majority-spin and minority-spin direction.

to a hole pocket centered at  $\Gamma$ , while bands 13 and 14 both yield  $\Gamma$ -centered hole sheets with necks at  $L$ . The sticking together of these last two bands along  $\Gamma X$  will be lifted if spin-orbit coupling is included.

The positron potential was derived from that of the electrons by sign reversal and omission of the exchange term. The positron  $\Gamma_1$  state was found to lie at 0.202 Ry. Figure 5(a) shows the positron density in the plane spanned by the vectors (1,0,0) and (0,1,1) which contains the empty lattice sites. There is a marked preference of the positrons for the vicinity of the empty sites. This is further illustrated by Fig. 5(b), which shows the effect of placing Ni atoms at the empty positions. In that way a

kind of model "Ni<sub>2</sub>MnSb" is obtained in which the muffin-tin potentials and the lattice constant, however, are those of NiMnSb. It is obvious that the positron density is much more evenly distributed in the model  $L 2_1$  compound which results in the  $\Gamma_1$  positron state being lifted to 0.454 Ry.

### C. Momentum density

In a 2D-ACAR experiment one measures the two-dimensional angular correlation  $N(p_y, p_z)$  between the annihilation photons

$$N(p_y, p_z) = C \int \rho^{2\gamma}(\mathbf{p}) dp_x, \quad (1)$$

where  $\rho^{2\gamma}(\mathbf{p})$  is the two-photon momentum density and  $C$  a constant depending on the experimental conditions. In a ferromagnet one can make use of the polarization of the positron beam to investigate the momentum density  $\rho_{\pm}^{2\gamma}(\mathbf{p})$  of the majority (+) and minority (-) electron-spin populations. In the independent-particle model  $\rho_{\pm}^{2\gamma}(\mathbf{p})$  is given by

$$\rho_{\sigma}^{2\gamma}(\mathbf{p}) = \sum_{\mathbf{k}, j} n_{j\sigma}(\mathbf{k}) \left| \int \exp(-i\mathbf{p}\cdot\mathbf{r}) \psi_{\mathbf{k}j\sigma}(\mathbf{r}) \phi(\mathbf{r}) d\mathbf{r} \right|^2. \quad (2)$$

Here  $\sigma = + (-)$  is the spin index, while  $\psi_{\mathbf{k}j\sigma}$  and  $\phi$  are the wave functions of the electron with wave vector  $\mathbf{k}$ , band index  $j$  and spin  $\sigma$ , and the positron in its ground state  $k_+ = 0$ , respectively. The occupation number  $n_{j\sigma}(\mathbf{k})$  indi-

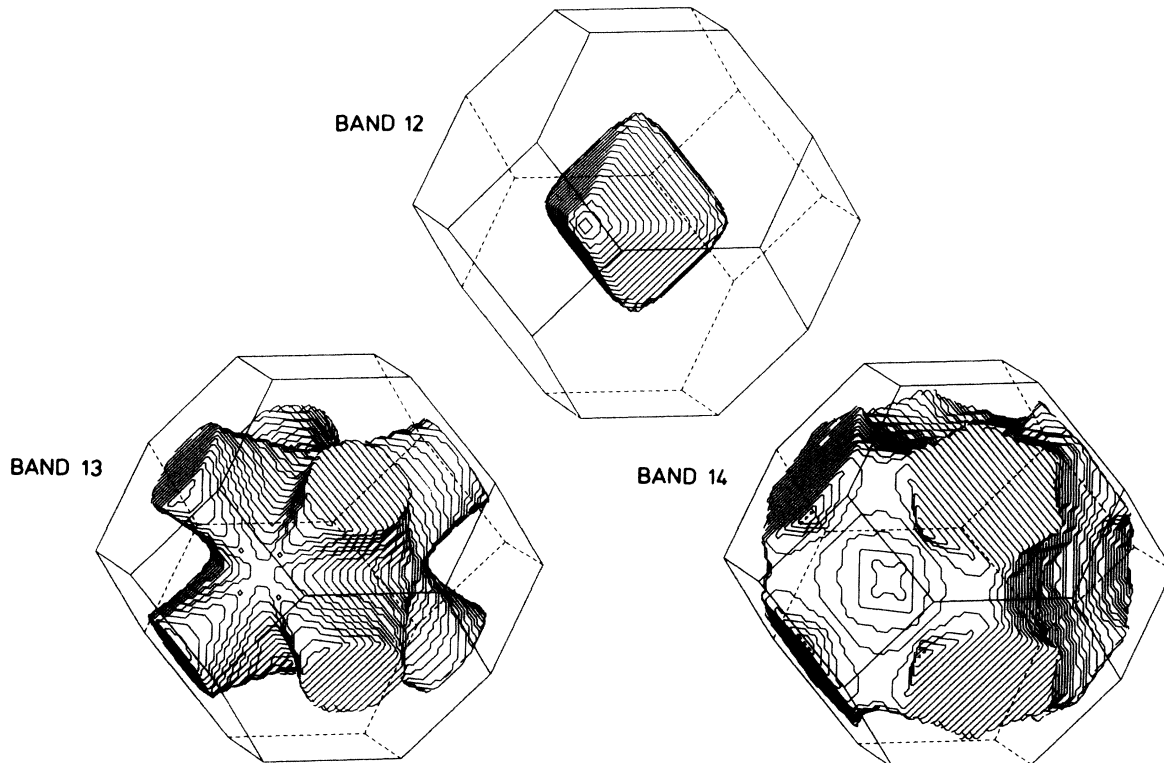


FIG. 4. The sheets of the Fermi surface for the majority-spin bands 12, 13, and 14.

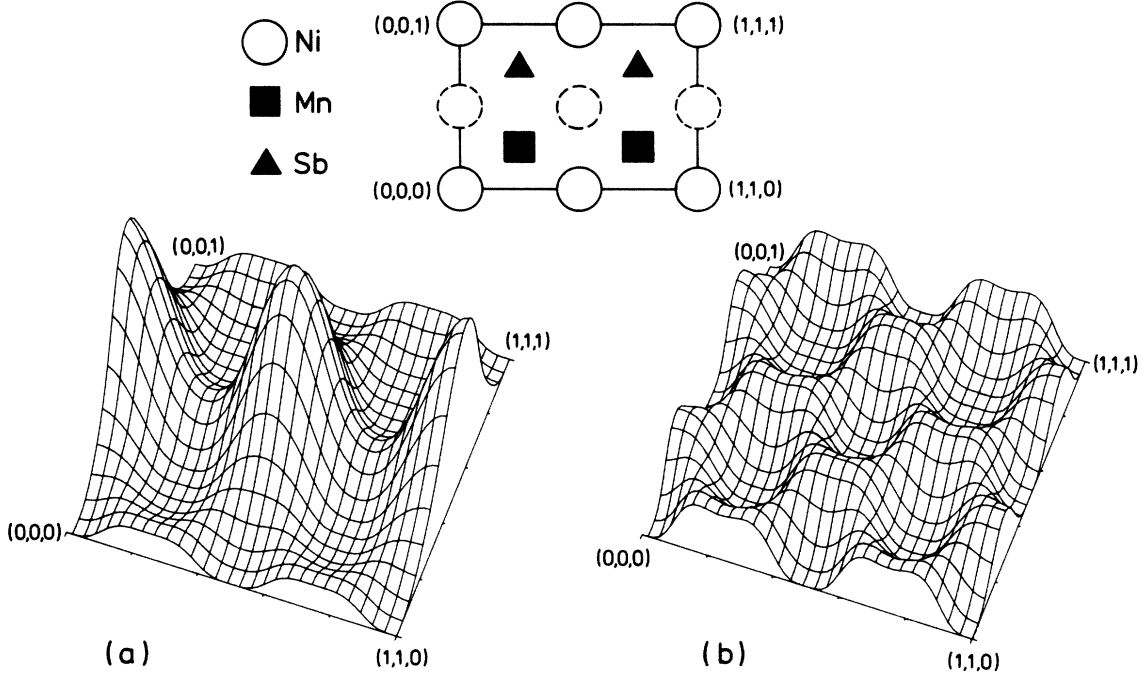


FIG. 5. (a) Positron probability density  $|\psi_+(\mathbf{r})|^2$  in the  $\{110\}$  planes of NiMnSb. The high peaks correspond to the empty lattice positions of the atoms (see inset). (b) Same for “Ni<sub>2</sub>MnSb,” obtained by placing additional Ni atoms at the empty lattice positions (dashed in the inset) of NiMnSb.

icates whether the state  $\mathbf{k}, j, \sigma$  is full or empty and is responsible for discontinuities in  $\rho_\sigma^{2\gamma}(\mathbf{p})$  at the Fermi surface, the so-called Fermi breaks.

Before engaging in a full calculation of the momentum density it is useful to investigate its symmetry properties. Owing to the translational symmetry of the crystal an electron with wave vector  $\mathbf{k}$  contributes to the momentum density  $\rho^{2\gamma}(\mathbf{p})$  at  $\mathbf{p}=\mathbf{k}+\mathbf{G}$ , where  $\mathbf{G}$  is a vector of the reciprocal lattice. The rotational symmetry, described by the point group  $T_d$ , results in a selection rule which allows one to locate the planes and lines of symmetry on which the momentum density corresponding to energy bands of a specific irreducible representation vanishes. Harthoorn and Mijnders<sup>22</sup> have collected the results of this selection rule in a set of tables for the simple-cubic [ $O_h^1 (Pm\bar{3}m)$ ], fcc [ $O_h^5 (Fm\bar{3}m)$ ], and bcc [ $O_h^9 (Im\bar{3}m)$ ] structures. Similar results for the point group  $T_d$ , based on the character tables given by Parmenter,<sup>23</sup> are presented in Table I. A comparison with the corresponding tables for the fcc ( $O_h^5$ ) structure shows that the lower symmetry of the  $T_d^2$  space group results in fewer restrictions on the observability of energy bands.

The spin-dependent momentum density of annihilation photon pairs  $\rho_\pm^{2\gamma}(\mathbf{p})$  was calculated using a plane-wave formulation of the KKR method.<sup>24</sup>  $\rho_\pm^{2\gamma}(\mathbf{p})$  was calculated for  $\sim 56\,000$   $\mathbf{p}$  vectors distributed over  $\frac{1}{48}$ th of a sphere of radius 4.0 a.u. Figures 6(a) and 6(b) show the total majority-spin momentum density  $\rho_+^{2\gamma}(\mathbf{p})$  and the contributions of individual bands to it along the  $\langle 001 \rangle$  and  $\langle 111 \rangle$  symmetry directions in momentum space. In accordance with Table I the Fermi breaks along the  $\langle 001 \rangle$  and  $\langle 111 \rangle$

directions are caused by band 12 ( $\Delta_1$  and  $\Lambda_1$ , respectively) crossing the Fermi level; those along  $\langle 110 \rangle$  (not shown here) are due to the  $\Sigma_1$  bands 12 and 13. Since band 13 contributes very little to  $\rho_+^{2\gamma}$  along  $\langle 110 \rangle$  the breaks due to that band are very small. There are no partially filled minority-spin bands. Hence  $\rho_-^{2\gamma}(\mathbf{p})$ , shown in Figs. 7(a) and 7(b), is everywhere continuous.<sup>25</sup>

To investigate how the uneven positron probability density affects the Fermi breaks in  $\rho_+^{2\gamma}$  we have also calculated the electron momentum density  $\rho_+(\mathbf{p})$  for Compton scattering, which follows from Eq. (2) by setting  $\phi=1$ . It is clear that  $\rho_+$ , shown in Fig. 8, is very similar to  $\rho_+^{2\gamma}$ . The Fermi breaks in the two distributions are of the same magnitude. This shows that the pronounced positron affinity to the empty lattice sites hardly affects the sampling of the partially filled bands by the positron.

### III. DISCUSSION

Our calculations show that the difference in character of the two electron-spin populations is clearly reflected in the spin-dependent momentum densities. As already mentioned, an experimental 2D-ACAR study of NiMnSb is in progress in our laboratory. Since in the experiment the positron beam is only partially polarized it is not possible to measure 2D-ACAR distributions for both spin directions separately. However, a difference measurement with an external magnetic field parallel ( $\uparrow$ ) or opposite ( $\downarrow$ ) to the positron polarization yields, after normalization of each of the measured distributions to unit volume under the distribution,

TABLE I. Observability of energy bands for momenta  $\mathbf{p}$  in the  $T_d^2$  lattice.  $\mathbf{p}$  stands for all vectors related by cubic symmetry, a minus sign indicates a zero contribution to  $\rho(\mathbf{p})$ , a plus sign a nonvanishing contribution to  $\rho(\mathbf{p})$ ,  $\bullet$  means there is no reciprocal-lattice vector connecting the wave vector  $\mathbf{k}$  of the symmetry type in the first column to this type of  $\mathbf{p}$  vector, and  $\xi$ ,  $\eta$ , and  $\zeta$  are all different and nonzero.

Energy band <sup>a</sup>	$p_x$	0	0	0	$\xi$	0	$\xi$	$\xi$
	$p_y$	0	0	$\xi$	$\xi$	$\xi$	$\eta$	$\eta$
	$p_z$	0	$\xi$	$\xi$	$\xi$	$\eta$	$\eta$	$\zeta$
$\Gamma_1$	+	+	+	+	+	+	+	+
$\Gamma_2$	-	-	-	-	-	+	-	+
$\Gamma_3$	-	+	+	-	+	+	+	+
$\Gamma_4$	-	+	+	+	+	+	+	+
$\Gamma_5$	-	-	+	-	+	+	+	+
$X_1, X_3$	$\bullet$	+	+	$\bullet$	+	+	+	+
$X_2, X_4$	$\bullet$	-	-	$\bullet$	+	-	+	+
$X_5$	$\bullet$	-	+	$\bullet$	+	+	+	+
$W_1, W_2, W_3, W_4$	$\bullet$	$\bullet$	$\bullet$	$\bullet$	+	+	+	+
$\Sigma_1, S_1$	$\bullet$	$\bullet$	+	$\bullet$	+	+	+	+
$\Sigma_2, S_2$	$\bullet$	$\bullet$	-	$\bullet$	+	-	+	+
$L_1, \Lambda_1$	$\bullet$	$\bullet$	$\bullet$	+	$\bullet$	+	+	+
$L_2, \Lambda_2$	$\bullet$	$\bullet$	$\bullet$	-	$\bullet$	-	+	+
$L_3, \Lambda_3$	$\bullet$	$\bullet$	$\bullet$	-	$\bullet$	+	+	+
$\Delta_1$	$\bullet$	+	$\bullet$	$\bullet$	+	+	+	+
$\Delta_2, \Delta_4$	$\bullet$	-	$\bullet$	$\bullet$	+	-	+	+
$\Delta_3$	$\bullet$	-	$\bullet$	$\bullet$	+	+	+	+
$V_1, V_2$	$\bullet$	$\bullet$	$\bullet$	$\bullet$	+	$\bullet$	+	+

<sup>a</sup>The symmetry labels are according to Ref. 19.

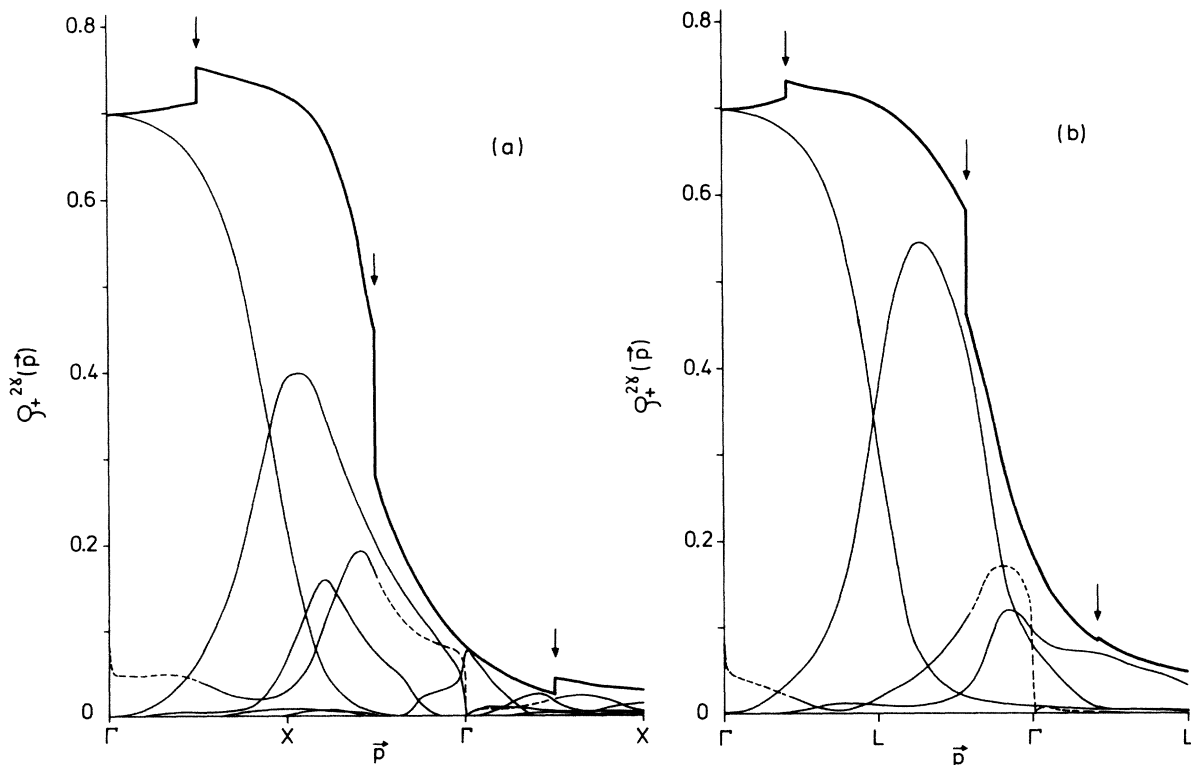


FIG. 6. (a) Momentum density of annihilation photon pairs along the direction  $\Gamma X$  for positrons annihilating with the majority-spin electrons in NiMnSb. The thin curves represent the contributions of the various bands. The dashed parts correspond to unoccupied states, thick curves give the total of all bands. The arrows indicate the Fermi breaks. (b) Same for  $\Gamma L$ .

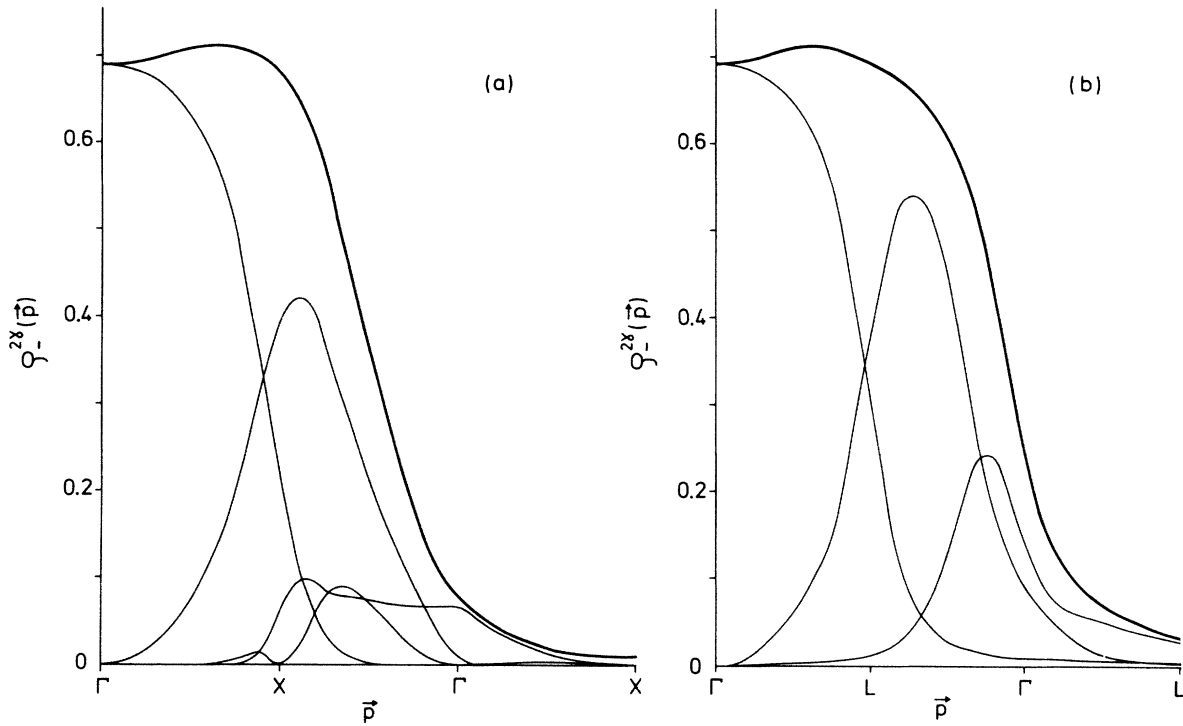


FIG. 7. (a) Momentum density of annihilation photon pairs for positrons annihilating with the minority-spin electrons along  $\Gamma X$ . (b) Same for  $\Gamma L$ .

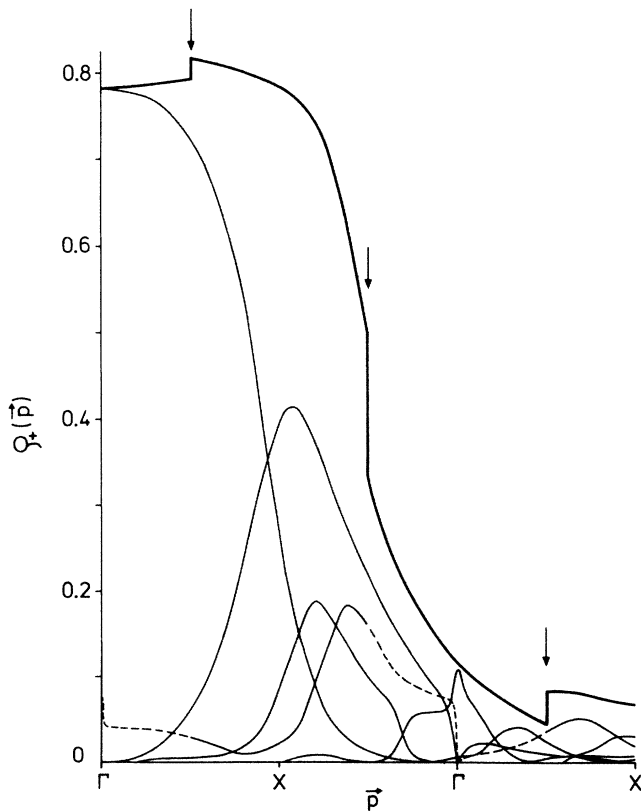


FIG. 8. Momentum density for Compton scattering of the majority-spin electrons along  $\Gamma X$ .

$$N_1^{2\gamma}(p_y, p_z) - N_1^{2\gamma}(p_y, p_z) = -P \left[ \frac{\rho_-(p_y, p_z)}{\rho_-} - \frac{\rho_+(p_y, p_z)}{\rho_+} \right], \quad (3)$$

where  $\rho_\sigma(p_y, p_z) = \int \rho_\sigma(\mathbf{p}) dp_x$  and  $\rho_\sigma = \int \rho_\sigma(\mathbf{p}) d\mathbf{p}$ , and  $P$  denotes the average polarization of the  $e^+$  beam.<sup>26</sup> If the  $e^+$  polarization is known it is possible to separate the contributions of the two spin populations to  $N^{2\gamma}$ .

A powerful tool in the analysis of the 2D-ACAR data is the Lock-Crisp-West (LCW) procedure.<sup>27</sup> This method of analysis, sometimes referred to as LCW folding, enhances Fermi-surface-related structure in the data at the expense of information connected with the wave functions. In its three-dimensional form<sup>28</sup> it is equivalent to summing the momentum densities at equivalent points  $\mathbf{p} = \mathbf{k} + \mathbf{G}$  in all Brillouin zones, i.e.,

$$h_\sigma(\mathbf{k}) = \sum_{\mathbf{G}} \rho_\sigma(\mathbf{k} + \mathbf{G}) = \sum_j n_{j\sigma}(\mathbf{k}) h_{j\sigma}(\mathbf{k}). \quad (4)$$

Here  $h_\sigma(\mathbf{k})$  is the LCW-folded total momentum density and  $h_{j\sigma}(\mathbf{k})$  the corresponding quantity for the  $j$ th band. If the positron wave function  $\phi(\mathbf{r}) = 1$  in Eq. (2), i.e., in the case of Compton scattering,  $h_{j\sigma}(\mathbf{k})$  is constant owing to wave-function normalization and hence  $h_\sigma(\mathbf{k}) \propto \sum_j n_{j\sigma}(\mathbf{k})$ , i.e., proportional to the total number of electrons with wave vector  $\mathbf{k}$ . Thus, for the minority-spin band one would expect  $h_-(\mathbf{k})$  to be independent of  $\mathbf{k}$  throughout the zone. However, as Rabou and Mijnen<sup>29,30</sup> have shown, for more realistic positron

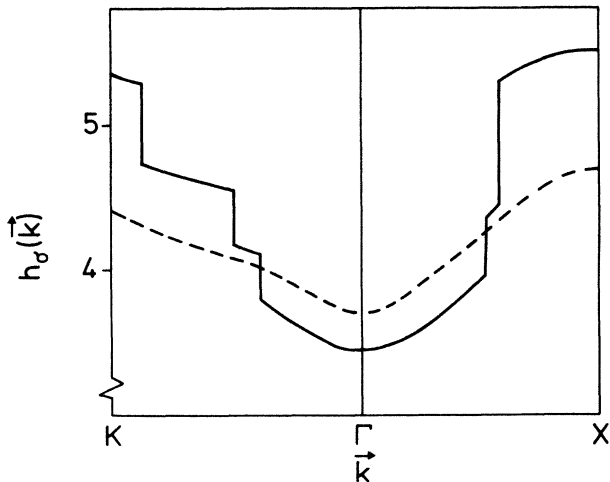


FIG. 9. Folded momentum density of annihilation photon pairs along  $\Gamma X$  and  $\Gamma K$  for annihilation with the majority-spin (solid) and minority-spin electrons (dashed).

wave functions substantial deviations can occur. These are also present in NiMnSb, as shown in Fig. 9: the folded minority-spin density  $h_{-}(\mathbf{k})$  is far from flat.

An interesting feature is visible in the momentum densities of the unoccupied states in bands 12 and 15 (for both positron annihilation and Compton scattering) near  $\mathbf{p}=\mathbf{0}$ . The density  $\rho_{12_{+}}(\mathbf{p})$  shows a very sharp peak which stems from the  $\Gamma_1$  level at 0.884 Ry. A corresponding sharp dip is found in  $\rho_{15_{+}}(\mathbf{p})$ . The detailed behavior of these densities is shown on an expanded  $|\mathbf{k}|$  scale along  $\Gamma X$  in Fig. 10(a). When added the peak and the dip just cancel. The corresponding bands are shown in Fig. 10(c). Examination of the compatibility relations for the  $T_d^2$  space group<sup>23</sup> and the selection rule in Table I provides an explanation for this peculiar behavior. Bands 12 and 15 are both  $\Delta_1$  bands with a nonzero momentum density along  $\langle 00\xi \rangle$ . They hybridize at  $\Gamma$ . Band  $15_{+}$  connects to the  $p$ -like  $\Gamma_4$  level which has a vanishing momentum density at  $\mathbf{p}=\mathbf{0}$ . Hence, a transfer of momentum density must take place from band 15 to band 12 (which connects to the  $s$ -like  $\Gamma_1$  level) as one approaches  $\mathbf{p}=\mathbf{0}$ . Since the two  $\Delta_1$  bands nearly touch at  $\Gamma$  (the gap between  $\Gamma_4$  and  $\Gamma_1$  is only 5 mRy) but diverge rapidly as  $|\mathbf{k}|$  increases, the momentum density transfer takes place very suddenly. This explains the sharpness of the peak and dip in Fig. 10(a). A similar situation is found for the minority-spin momentum densities  $\rho_{12_{-}}(\mathbf{p})$  and  $\rho_{15_{-}}(\mathbf{p})$ , but here the order of the levels at  $\Gamma$  is reversed. Hence, the peak is found in  $\rho_{15_{-}}(\mathbf{p})$  and the dip in  $\rho_{12_{-}}(\mathbf{p})$ . Also, these features are not quite as sharp as for the majority-spin band because the hybridization of the two minority-spin  $\Delta_1$  bands is stronger and hence the momentum density transfer is more gradual. Since the LCW theorem must hold for each band separately,  $\rho_{12_{\pm}}(\mathbf{p})$  and  $\rho_{15_{\pm}}(\mathbf{p})$  must also be affected in the vicinity of other  $\Gamma$  points in  $\mathbf{p}$  space. It explains for instance the sudden drop in  $\rho_{12_{+}}(\mathbf{p})$

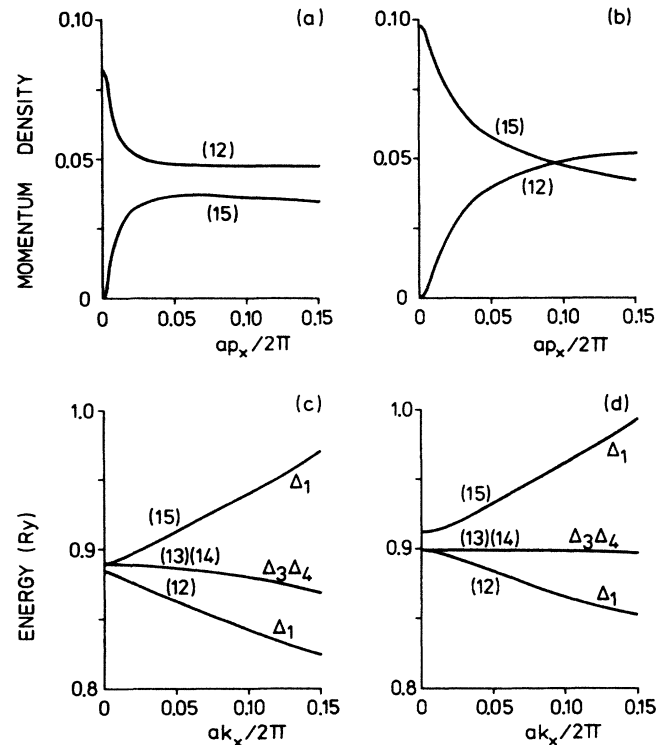


FIG. 10. Momentum density of annihilation photon pairs and band structure for bands 12 to 15 along  $\Gamma X$  in the neighborhood of  $\mathbf{p}=\mathbf{0}$  for (a),(c) the majority-spin electrons and (b),(d) the minority-spin electrons. Band indices are given within parentheses.

near  $\mathbf{p}=(2\pi/a)(0,0,2)$  visible in Fig. 6(a). Indeed, LCW folding of the momentum densities in band 12 and band 15 for Compton scattering, involving summation over various numbers of reciprocal-lattice vectors up to a maximum of 3000, yields a result which tends to unity for each of these bands over the interval  $0 \leq ak_x/2\pi \leq 0.15$  studied. Obviously, experimental observation of the sharp features described here is impossible in NiMnSb since the electron states from which they originate are empty. If *both* hybridizing bands are situated below the Fermi level these features are equally unobservable as they cancel in the total momentum density  $\rho(\mathbf{p})$ . Only when the Fermi level lies between the two bands can structure like this occur in  $\rho(\mathbf{p})$ .

#### ACKNOWLEDGMENTS

The authors wish to thank Dr. R. A. de Groot for supplying the potentials and for useful discussions, and Dr. M. S. Methfessel for making the computer program for the density-of-states calculation available to us. This work is part of the research program of the Stichting Fundamenteel Onderzoek der Materie (Foundation for Fundamental Research on Matter) and was made possible by financial support from the Nederlandse Organisatie voor Zuiver-Wetenschappelijk Onderzoek (Netherlands Organization for the Advancement of Pure Research).

- <sup>1</sup>R. A. de Groot, F. M. Mueller, P. G. van Engen, and K. H. J. Buschow, *Phys. Rev. Lett.* **50**, 2024 (1983).
- <sup>2</sup>R. A. de Groot, F. M. Mueller, P. G. van Engen, and K. H. J. Buschow, *J. Appl. Phys.* **55**, 2151 (1984).
- <sup>3</sup>J. Kübler, *Physica (Utrecht)* **127B**, 257 (1984).
- <sup>4</sup>R. A. de Groot and K. H. J. Buschow, *J. Magn. Magn. Mater.* **54-57**, 1377 (1986).
- <sup>5</sup>K. Watanabe, *Trans. Jpn. Inst. Met.* **17**, 220 (1976).
- <sup>6</sup>P. G. van Engen, K. H. J. Buschow, R. Jongebreur, and M. Erman, *Appl. Phys. Lett.* **42**, 202 (1983).
- <sup>7</sup>K. H. J. Buschow, P. G. van Engen, and R. Jongebreur, *J. Magn. Magn. Mater.* **38**, 1 (1983).
- <sup>8</sup>M. H. Kryder, *J. Appl. Phys.* **57**, 3913 (1985).
- <sup>9</sup>P. G. van Engen, Ph.D. thesis, Technological University Delft, 1983.
- <sup>10</sup>P. A. M. van der Heide, W. Baelde, R. A. de Groot, A. R. de Vroomen, P. G. van Engen, and K. H. J. Buschow, *J. Phys. F* **15**, L75 (1985).
- <sup>11</sup>G. L. Bona, F. Meier, M. Taborelli, E. Bucher, and P. H. Schmidt, *Solid State Commun.* **56**, 391 (1985).
- <sup>12</sup>S. Berko, in *Positron Annihilation*, edited by R. R. Hasiguti and K. Fujiwara (Japan Institute of Metals, Sendai, 1979), p. 65.
- <sup>13</sup>S. Berko, in *Positron Annihilation*, edited by A. T. Stewart and L. O. Roellig (Academic, New York, 1967), p. 61.
- <sup>14</sup>S. Berko and A. P. Mills, *J. Phys. (Paris) Colloq.* **32**, C1-287 (1971).
- <sup>15</sup>R. N. West, in *Positrons in Solids*, edited by P. Hautojärvi (Springer, Berlin, 1979), p. 89.
- <sup>16</sup>R. B. Helmholtz, R. A. de Groot, F. M. Mueller, P. G. van Engen, and K. H. J. Buschow, *J. Magn. Magn. Mater.* **43**, 249 (1984).
- <sup>17</sup>F. Heusler, *Verh. Dtsch. Phys. Ges.* **5**, 219 (1903).
- <sup>18</sup>T. Takeda, *Z. Phys. B* **32**, 43 (1978).
- <sup>19</sup>S. C. Miller and W. F. Love, *Tables of Irreducible Representations of Space Groups and Co-Representations of Magnetic Space Groups* (Pruett, Boulder, 1967), p. 386.
- <sup>20</sup>C. Herring, *Phys. Rev.* **52**, 361 (1937).
- <sup>21</sup>M. S. Methfessel, M. H. Boon, and F. M. Mueller, *J. Phys. C* **16**, L949 (1983).
- <sup>22</sup>R. Harthoorn and P. E. Mijndarends, *J. Phys. F* **8**, 1147 (1978).
- <sup>23</sup>R. H. Parmenter, *Phys. Rev.* **100**, 573 (1955).
- <sup>24</sup>P. E. Mijndarends and L. P. L. M. Rabou, *J. Phys. F* **16**, 483 (1986).
- <sup>25</sup>S. Berko and J. S. Plaskett, *Phys. Rev.* **112**, 1877 (1958).
- <sup>26</sup>L. P. L. M. Rabou, P. E. Mijndarends, and H. Neddermeyer, *Positron Annihilation*, edited by P. G. Coleman, S. C. Sharma, and L. M. Diana (North-Holland, Amsterdam, 1982), p. 257.
- <sup>27</sup>D. G. Lock, V. H. C. Crisp, and R. N. West, *J. Phys. F* **3**, 561 (1973).
- <sup>28</sup>S. Berko, in *Positron Solid-State Physics*, edited by W. Brandt and A. Dupasquier (North-Holland, Amsterdam, 1983), p. 64.
- <sup>29</sup>L. P. L. M. Rabou and P. E. Mijndarends, *Solid State Commun.* **52**, 933 (1985); **53**, (7), i (1985).
- <sup>30</sup>L. P. L. M. Rabou and P. E. Mijndarends, in *Positron Annihilation*, edited by P. C. Jain, R. M. Singru, and K. P. Gopinathan (World Scientific, Singapore, 1985), p. 68.